

The Stability of a Cantilever Beam Subjected to One-Dimensional Leakage Flow

Hiroshi NAGAKURA, Shigehiko KANEKO
University of Tokyo, Tokyo, Japan

ABSTRACT

The stability of a cantilever beam subjected to one-dimensional leakage flow is studied both theoretically and experimentally. It is clarified that in the case that the beam is clamped at the upstream end, the system loses stability by coupled-mode flutter, on the other hand, in the case that the beam is clamped at the downstream end, the system first loses stability by divergence and successively loses stability by flutter with increasing flow velocity.

1 INTRODUCTION

Leakage-flow-induced vibrations have been studied quite intensively particularly in connection with the instability of nuclear power plant components. Inada and Hayama [1,2] studied the fluid-dynamic force acting on the vibrating wall in a narrow passage and examined the mechanism of instability due to one-dimensional leakage flow, however, in this study, the case of an elastically supported rigid plate was analyzed and the instability of flexible structures were not considered.

In this paper, to study the mechanism of leakage-flow-induced instability of flexible structures, the stability of a cantilever beam subjected to one-dimensional leakage flow is analyzed and compared with experimental results.

2 ANALYSIS

2.1 System definition and assumptions

Fig.1 shows the system under consideration. It consists of a cantilever plate located in parallel with rigid walls. The plate is clamped either at the upstream end or at the downstream end. The x axis coincides with the center line of the channel. Gap width H_0 is much smaller than the plate length L , which is identical to the passage length. It is assumed that fluid flows almost parallel to the x axis and $\partial P/\partial z=0$. Assuming that the plate and the flow are uniform in the y direction, we regard the plate as a beam.

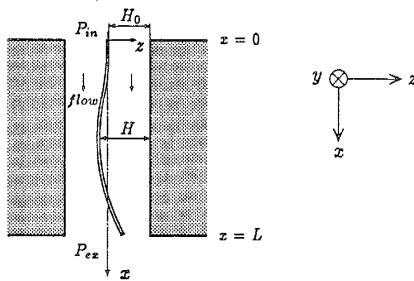


Fig. 1. Schematic diagram of the system.

2.2 Basic equations

The equation of motion for the beam is written as

$$m \frac{\partial^2 w}{\partial t^2} + \nu \frac{\partial w}{\partial t} + EI \frac{\partial^4 w}{\partial x^4} = F(x, t), \quad (1)$$

where F is the fluid force per unit length. Integrating the equations of motion and continuity of fluid in a narrow passage with respect to z yields [1]

$$\frac{\partial Q}{\partial t} + \frac{\partial}{\partial x} \left(\frac{Q^2}{H} \right) = -\frac{H}{\rho_a} \frac{\partial P}{\partial x} - \frac{\lambda Q^2}{4H^2}, \quad \frac{\partial Q}{\partial x} + \frac{\partial H}{\partial t} = 0, \quad (2, 3)$$

where H , P , Q , ρ_a and λ denote gap width, pressure, flow rate per unit width, density of fluid and pressure loss coefficient of the passage, respectively. Boundary conditions at the inlet and the outlet of the passage are

$$P(0, t) = P_{in} - \xi_{in} \frac{\rho_a Q^2(0, t)}{2H^2(0, t)}, \quad P(L, t) = P_{ex} + \xi_{ex} \frac{\rho_a Q^2(L, t)}{2H^2(L, t)}, \quad (4, 5)$$

where P_{in} and P_{ex} are the constant pressure just outside the inlet and outlet, ξ_{in} and ξ_{ex} are the pressure loss coefficients at the inlet and outlet.

2.3 The stability of infinitesimal oscillations

Assuming the solution of Eq.(1) in the form of

$$w(x, t) = \sum_{n=1}^{\infty} \phi_n(x) h_n(t), \quad (6)$$

where h_n is the perturbed displacement of the n th mode of the beam and ϕ_n is the eigenfunction of a cantilever, gap width of the right-hand side passage can be written as

$$H(x, t) = H_0 + \sum_{n=1}^{\infty} \phi_n(x) h_n(t). \quad (7)$$

Pressure and flow rate per unit width in the right-hand side passage can be written as

$$P(x, t) = \bar{P}(x) + p(x, t), \quad Q(x, t) = \bar{Q} + q(x, t), \quad (8, 9)$$

where \bar{P} and \bar{Q} denote the mean value, p and q denote structural motion induced perturbations. Because of the symmetry, the motion-induced perturbations in the left-hand side passage have same amplitudes but opposite phases to the right ones. Thus the fluid force acting on the beam is twice as large as pW , where W is the width of the plate. Considering the above and substituting Eq.(6) into Eq.(1) yield

$$\sum_{n=1}^{\infty} \left(\frac{d^2 h_n}{dt^2} + 2\zeta_n \Omega_n \frac{dh_n}{dt} + \Omega_n^2 h_n \right) \phi_n(x) = \frac{2p}{\rho_b t}, \quad (10)$$

where Ω_n is the n th natural circular frequency of the beam, ζ_n is the damping ratio of the n th mode of the beam, and ρ_b is the density of beam. Substituting Eqs.(7)~(9) into Eqs.(2)~(5), and neglecting the second and higher order terms of the perturbations, we obtain

$$\frac{\partial p}{\partial x} = -\frac{\rho_a}{H_0} \left\{ \frac{\partial q}{\partial t} + \frac{\bar{Q}}{H_0 L} 2\beta\gamma q + \frac{2\bar{Q}}{H_0} \frac{\partial q}{\partial x} - \frac{\bar{Q}^2}{H_0^2} \sum_{n=1}^{\infty} \left(\frac{3\beta\phi_n}{L} + \frac{d\phi_n}{dx} \right) h_n \right\}, \quad (11)$$

$$\frac{\partial q}{\partial x} + \sum_{n=1}^{\infty} \phi_n \frac{dh_n}{dt} = 0, \quad (12)$$

$$p(0, t) = -\xi_{in} \frac{\rho_a}{H_0} \left\{ \frac{\bar{Q}}{H_0} q(0, t) - \frac{\bar{Q}^2}{H_0^2} \sum_{n=1}^{\infty} \phi_n(0) h_n \right\}, \quad (13)$$

$$p(L, t) = \xi_{ex} \frac{\rho_a}{H_0} \left\{ \frac{\bar{Q}}{H_0} q(L, t) - \frac{\bar{Q}^2}{H_0^2} \sum_{n=1}^{\infty} \phi_n(L) h_n \right\}, \quad (14)$$

where

$$\beta = \frac{\bar{\lambda}L}{4H_0}, \quad \gamma = 1 + \frac{\bar{Q}}{2\bar{\lambda}} \left(\frac{d\lambda}{dQ} \right)_{Q=\bar{Q}} \quad (15)$$

The Laplace transform of Eqs.(11)~(14) yield

$$P(x, \bar{s}) = -\frac{\rho_a L^2}{H_0} \sum_{n=1}^{\infty} \left\{ m_n \bar{s}^2 + \left(c_n + \frac{c'_n}{1 + \frac{H_0 L}{\bar{Q}} T} \right) \frac{\bar{Q}}{H_0 L} \bar{s} + \left(k_n + \frac{k'_n}{1 + \frac{H_0 L}{\bar{Q}} T} \right) \left(\frac{\bar{Q}}{H_0 L} \right)^2 \right\} H_n(\bar{s}), \quad (16)$$

where \bar{s} and T denote the Laplace transform operator and the nondimensional time constant, $P(x, \bar{s})$ and $H_n(\bar{s})$ denote the Laplace transform of $p(x, t)$ and $h_n(t)$, respectively. m_n, c_n, k_n, c'_n and k'_n are nondimensional functions of x .

Taking the Laplace transform of Eq.(10) with Eq.(16), we obtain

$$\sum_{n=1}^{\infty} (s^2 + 2\zeta_n \omega_n s + \omega_n^2) \phi_n(x) H_n = -\frac{2\rho_a L^2}{\rho_b t H_0} \sum_{n=1}^{\infty} \left\{ m_n s^2 + \left(c_n + \frac{c'_n}{1 + sT/u} \right) us + \left(k_n + \frac{k'_n}{1 + sT/u} \right) u^2 \right\} H_n, \quad (17)$$

where s denotes the Laplace transform operator with respect to $\tau = \Omega_0 t$, where $\Omega_0 = (EI/mL^4)^{1/2}$, and $u = \bar{Q}/\Omega_0 H_0 L$, which is referred to as the non-dimensional flow velocity. Multiplying Eq.(17) by $\phi_m(x)$ and integrating over the length of the beam yield

$$(s^2 + 2\zeta_m \omega_m s + \omega_m^2) H_m = -\frac{2\rho_a L^2}{\rho_b t H_0} \sum_{n=1}^{\infty} \left\{ m_{mn} s^2 + \left(c_{mn} + \frac{c'_{mn}}{1 + sT/u} \right) us + \left(k_{mn} + \frac{k'_{mn}}{1 + sT/u} \right) u^2 \right\} H_n, \quad (18)$$

where $m_{mn} = \int_0^L \phi_m m_n dx / \int_0^L \phi_m^2 dx$, and c_{mn}, k_{mn}, c'_{mn} and k'_{mn} are defined in the same manner as m_{mn} . Truncating the sum at r , Eq.(18) can be written in matrix form as

$$\begin{bmatrix} s^2 + 2\zeta_m \omega_m s + \omega_m^2 & & 0 \\ & \ddots & \\ 0 & & s^2 + 2\zeta_r \omega_r s + \omega_r^2 \end{bmatrix} \begin{Bmatrix} H_1 \\ \vdots \\ H_r \end{Bmatrix} = -\frac{2\rho_a L^2}{\rho_b t H_0} \begin{bmatrix} P_{11}(s) & \cdots & P_{1r}(s) \\ \vdots & \ddots & \vdots \\ P_{r1}(s) & \cdots & P_{rr}(s) \end{bmatrix} \begin{Bmatrix} H_1 \\ \vdots \\ H_r \end{Bmatrix}, \quad (19)$$

where $P_{mn}(s)$ corresponds to the term in the curly brackets in Eq.(18). The matrix in the left-hand side in Eq.(19) becomes diagonal due to the orthogonality of the eigenfunctions of the beam, on the other hand, the matrix in the right-hand side becomes dense because the modes of the beam are coupled to each other by the fluid.

The characteristic equation of the system is given by $\det A = 0$, where A denotes the matrix obtained by transposing the right-hand side of Eq.(19) to left-hand side. The system becomes unstable when at least one characteristic root has positive real part, and if the corresponding imaginary part is positive, the system loses stability by flutter, and if it is zero, the system loses stability by divergence.

2.4 Characteristics of the flutter type instability

In this section, it is shown that two types of flutter, i.e. coupled-mode-flutter and single-degree-of-freedom flutter can be classified by examining the increment of total energy during one cycle of vibration. Considering the case of neutral stability and taking $s = i\omega$, Eq.(19) can be rewritten as

$$(Ms + Ma) \ddot{\mathbf{H}} + (Cs + Ca) \dot{\mathbf{H}} + (Ks + Ka) \mathbf{H} = \mathbf{0} \quad (20)$$

where Ms, Cs and Ks denote structural mass, damping and stiffness matrix, Ma, Ca and Ka denote fluid-dynamic mass, damping and stiffness matrix, respectively, and $\mathbf{H} = \{h_1, \dots, h_r\}^T$ denotes the displacement vector. The increment of total energy during one cycle of vibration is expressed as

$$\Delta E = - \int_0^{2\pi/\omega} \left\{ \dot{\mathbf{H}}^T (Ms + Ma) \ddot{\mathbf{H}} + \dot{\mathbf{H}}^T (Cs + Ca) \dot{\mathbf{H}} + \dot{\mathbf{H}}^T (Ks + Ka) \mathbf{H} \right\} d\tau. \quad (21)$$

ΔE has two components, i.e. the direct term and the cross term. In the case of neutral stability, the direct term and the cross term have same magnitude with opposite sign. When the direct term is positive, the type of flutter is single-degree-of-freedom flutter, on the other hand, when the cross term is positive, it shows coupled-mode-flutter.

3 COMPARISON BETWEEN EXPERIMENTAL AND CALCULATED RESULTS

3.1 Experiment

Experiments were conducted with cantilevered plate in air-flow. Fig. 2 shows the test section of the experimental apparatus. The plate made of copper is clamped at the top end, and air flows either downwards or upwards in the narrow passages. Displacement of the plate is measured at the bottom end of the plate by a photonic sensor.

3.2 Calculation

Calculations were conducted by truncating the sum at $r=6$. The damping ratio of each mode is assumed as $\zeta_n=0.01$.

3.3 In the case that the beam is clamped at the upstream end

Experimental results of the amplitude and the frequency are plotted against the flow velocity in two representative cases and shown in Fig. 3. With increasing flow velocity, the amplitude becomes large abruptly at a certain flow velocity, which is referred to as the critical flow velocity. In Fig. 3(b), two unstable modes exist and the lower mode instability is followed by the higher mode instability.

The roots of the characteristic equation are calculated in two cases and results are shown in Fig. 4(a) and 4(b), which correspond to experimental results shown in Fig. 3(a) and 3(b), respectively. The characteristic roots are plotted in the s -plane as a function of the nondimensional flow velocity U/U_{cr} . The dashed-lines in these figures denote the natural circular frequencies of the first four modes of a cantilever beam without fluid. The system loses stability when at least one characteristic root has positive real part. These figures well illustrate the behaviour of the system.

Fig. 5(a) and 5(b) show the effects of gap width. The frequencies at the onset of instability increase stepwise as gap width becomes narrower. Agreement between experimental and theoretical results is reasonably good.

Fig. 6(a) shows the nondimensional circular frequency $\omega=2\pi f/\Omega_0$ as a function of the nondimensional parameter $\rho_a L^2/\rho_b t H_0$, which represents the ratio of added mass to structural mass. It is shown that as this parameter is increased, the higher mode instability occurs. Fig. 6(b) shows the nondimensional critical flow velocity $u_{cr}=U_{cr}/\Omega_0 L$ as a function of the parameter $\rho_a L^2/\rho_b t H_0$. It is shown that the critical flow velocities for higher mode instability is larger than those for lower one.

The mode shape of the system on the neutral stability is calculated and two components of the increment of total energy during one cycle of the vibration is calculated. It is found that the type of flutter is coupled-mode flutter.

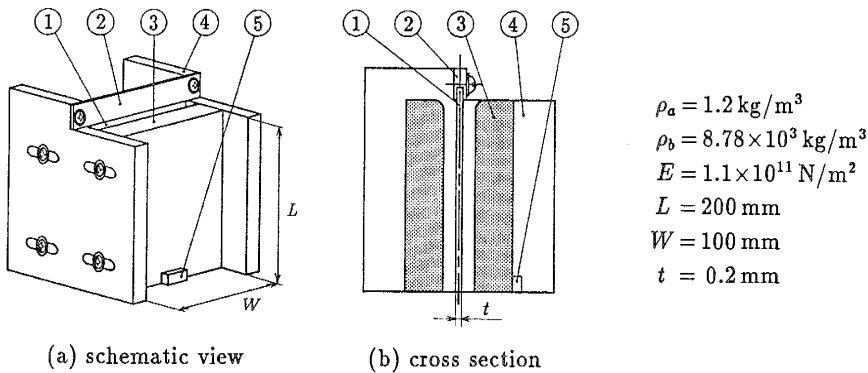


Fig. 2. Test section, 1: plate, 2: support, 3: wall of passage, 4: side wall of passage, 5: photonic sensor.

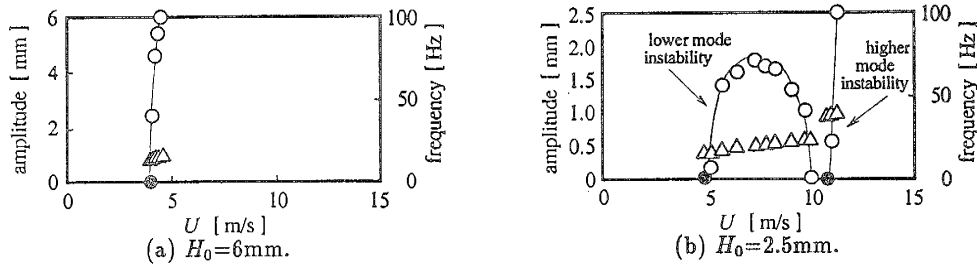


Fig. 3. Amplitude (○) and frequency (△) as a function of flow velocity. ● denotes the onset of instability.

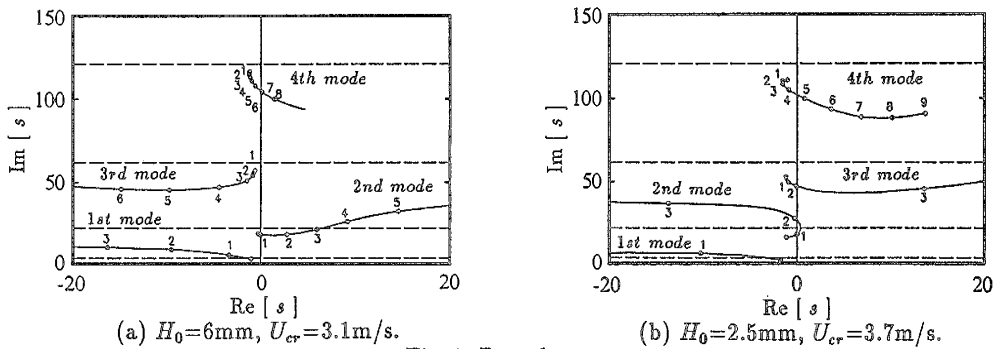


Fig. 4. Root locus.

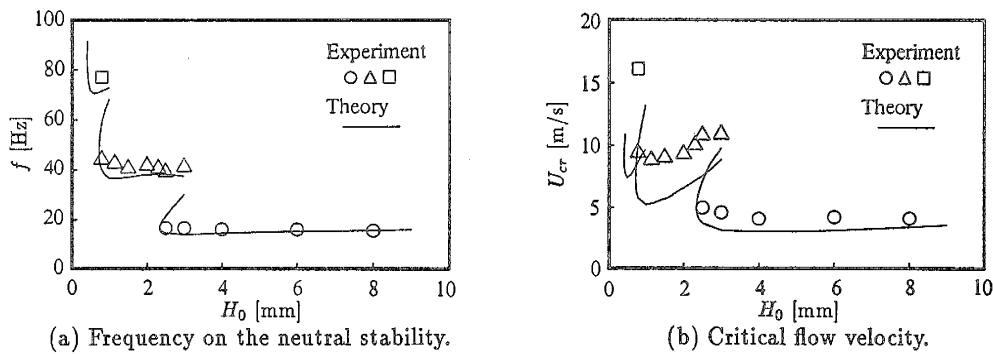


Fig. 5. Effects of gap width.

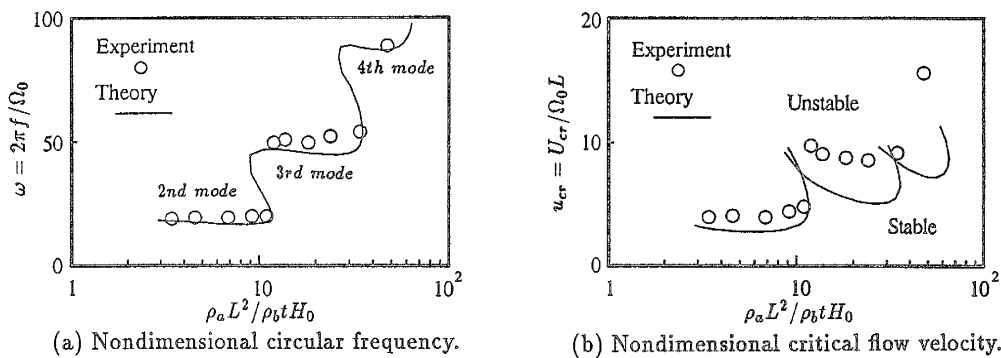


Fig. 6. Effects of parameter $\rho_a L^2 / \rho_b t H_0$.

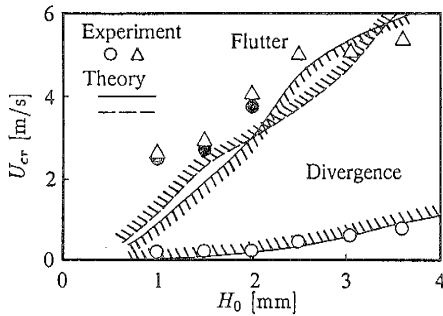


Fig. 7. Critical flow velocity versus gap width. ○ and △ denote the onset of divergence and flutter, respectively. When $H_0 \leq 2\text{mm}$, the system became stable at ●.

3.4 In the case that the beam is clamped at the downstream end

Fig. 7 shows the critical flow velocity as a function of gap width. The system first loses stability by divergence and successively loses stability by flutter. Agreement between experimental and theoretical results of critical flow velocity for divergence is good. In the experiments, post-divergence behaviours of the system were classified in the following two cases, (i) the system became stable and then unstable by flutter, (ii) the system successively lost stability by large amplitude flutter without regaining stability. Experimental results for flutter are in agreement with theoretical ones so far as the assumption of small oscillation is valid.

The critical flow velocities for divergence calculated by truncating the sum at $r=1$ were almost same as those by truncating the sum at $r=6$, so we regard the system as single-degree-of-freedom system. Under this assumption, the condition for divergence can be written simply as

$$\omega_1^2 + 2 \frac{\rho_a L^2}{\rho_b t H_0} (k_{11} + k'_{11}) u^2 < 0, \quad (22)$$

where $\omega_1=3.516$ the nondimensional first natural circular frequency of a cantilever beam, $k_{11} + k'_{11}$ is the (1,1) component of fluid-dynamic stiffness matrix.

4 CONCLUSIONS

The stability of a cantilever beam subjected to one-dimensional leakage flow is investigated both theoretically and experimentally. In the case that the beam is clamped at the upstream end, the system loses stability by coupled-mode flutter. As the ratio of added mass to structural mass becomes larger, higher mode instability occurs. In the case that the beam is clamped at the downstream end, the system first loses stability by divergence, and successively loses stability by flutter with increasing flow velocity.

REFERENCES

1. INADA, F. and HAYAMA, S., 1990, "A study on leakage-flow-induced vibrations. Part 1: Fluid-dynamic forces and moments acting on the walls of a narrow tapered passage." *Journal of Fluids and Structures* 4, 395-412.
2. INADA, F. and HAYAMA, S., 1990, "A study on leakage-flow-induced vibrations. Part 2: Stability analysis and experiments for two-degree-of-freedom systems combining translational and rotational motions." *Journal of Fluids and Structures* 4, 413-428.